Tunable Real Space Transfer Oscillator by Delayed Feedback Control of Chaos

D. P. Cooper and E. Schöll

Institut für Theoretische Physik, Technische Universität Berlin, Hardenbergstr. 36, D-10623 Germany

Z. Naturforsch. **50a**, 117–124 (1995); received November 5, 1994

It is demonstrated numerically that by using Pyragas' method of chaos self-control a stable semiconductor oscillator can be designed based on driven real-space transfer oscillations in a modulation-doped heterostructure. By application of a small time-continuous delayed feedback voltage control signal, different unstable periodic orbits embedded in the chaotic attractor can be stabilized. Thus different modes of self-generated periodic voltage oscillations can be selected by choosing an appropriate delay time. This provides tunability to different discrete frequencies.

PACS numbers: 05.45.+b, 72.20 Ht.

1. Introduction

Recent theoretical and experimental efforts to control chaos in physical systems, that is, to convert chaotic behaviour to a periodic time dependence, have shed a new light on the role of chaotic dynamics in view of practical applications. It turns out that the presence of chaos, when controllable, can be advantageous. We demonstrate this for the case of electrical instabilities in the regime of nonlinear hot carrier transport [1–3], which can be used in semiconductor devices as microwave oscillators [4]. By applying a small self-control, we achieve stable and tunable regular oscillations. Our underlying principle is based upon the observation that any chaotic attractor of a nonlinear dynamic system contains an infinite dense set of unstable periodic orbits (UPO). As shown by Ott, Grebogi and Yorke (OGY) [5], any of these UPOs may be stabilized by applying a small time-dependent perturbation to the control parameter of the system such that the trajectories are thrown onto the stable manifold of the particular UPO. Thus the inherent chaotic dynamics create a flexible situation in which it is possible to choose between quite different periodic orbits using only a small control.

A disadvantage of the OGY method is that the feedback control is applied only at discrete points of time given by the return times of the Poincaré map of the dynamic flow, which has to be computed for this purpose. The method can thus stabilize only those UPOs whose largest Lyapunov exponent is small compared to the reciprocal time interval between the parameter changes. A novel, powerful method of chaos control by a small time-continuous perturbation which does not require on-line computations has been proposed by Pyragas [6]. The stabilization of UPOs is achieved by adding a delayed self-controlled feedback to one of the dynamic equations. Here we numerically demonstrate that a simple and stable tunable semiconductor oscillator can be built on this principle.

Reprint requests to Prof. E. Schöll.

2. Model

We consider nonlinear charge transport parallel to the layers of the modulation-doped GaAs/$Al_xGa_{1-x}As$ heterostructure schematically shown in Figure 1(a). In experiments the system displays N-shaped negative differential conductivity (NNDC) [7], ac-driven current oscillations [8] and spontaneous oscillations under dc bias [9–12]. The heterostructure consists of a GaAs layer of width L_1 and an $Al_xGa_{1-x}As$ layer of width L_2. At the layer interface the conduction band displays a discontinuity ΔE_C as shown in Figure 1(b). The $Al_xGa_{1-x}As$ layer is heavily n-doped with donor density N_D. In thermodynamical equilibrium the donors are ionized, and the valence electrons, separated from their parent donors in the $Al_xGa_{1-x}As$ layer, fall into the lower potential of the GaAs well. There they experience strongly reduced impurity scat-

0932-0784 / 95 / 0200-0117 $ 06.00 © – Verlag der Zeitschrift für Naturforschung, D-72027 Tübingen

Bereitgestellt von | provisional account
Angemeldet
Heruntergeladen am | 14.11.18 14:53

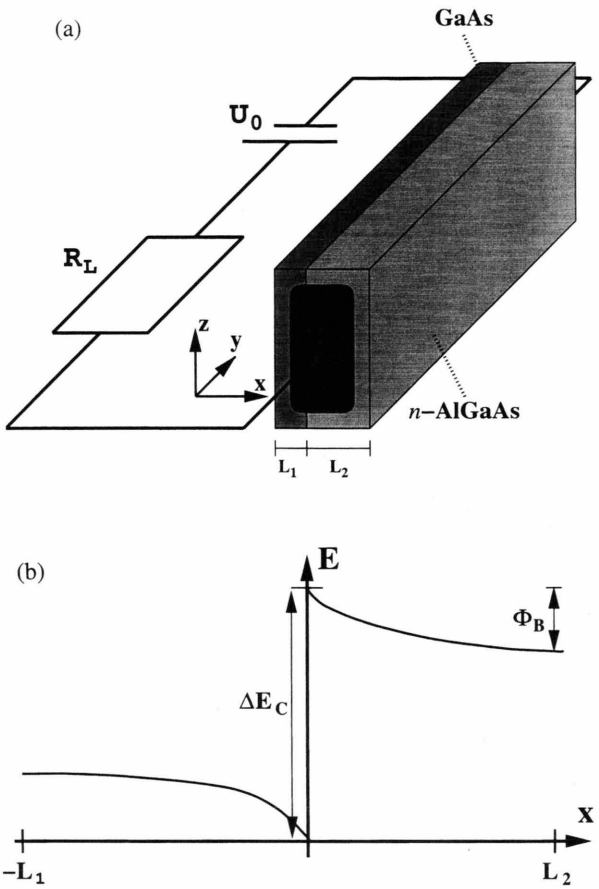

Fig. 1. (a) The modulation doped GaAs/$Al_xGa_{1-x}As$ heterostructure in an external circuit with load resistance R_L and bias voltage U_0. L_1 and L_2 are the heterolayer widths. (b) Energy-band diagram versus the vertical coordinate x. The conduction band has a discontinuity ΔE_C at the interface, and band bending in the $Al_xGa_{1-x}As$ layer results in the potential Φ_B.

tering and the mobility μ_1 is high. The resulting space charge in the $Al_xGa_{1-x}As$ gives rise to band bending and the interface potential barrier Φ_B.

Application of an electric field parallel to the layer interface induces carrier heating, and for a field $\mathscr{E}_\parallel > 2\,\mathrm{kV/cm}$ thermionic emission of electrons across the barrier into the $Al_xGa_{1-x}As$ is possible. This leads to an increased carrier density n_2 in the $Al_xGa_{1-x}As$, where the electron mobility μ_2 is much lower due to strongly enhanced impurity scattering, and a reduced density n_1. Thus for the longitudinal current, increasing the voltage results in a reduced average mobility, and there exists a regime of negative differential conductivity. The current-voltage characteristic has the shape of an N, which is in analogy to the Gunn effect, where the underlying physical mechanism is the transfer of electrons from a state in momentum space with high mobility to a state of low mobility (intervalley transfer in k-space).

A physical mechanism for self-generated current oscillations under dc bias conditions has been proposed [13], based upon the coupled nonlinear dynamics of real-space electron transfer and of the space-charge in the doped $Al_xGa_{1-x}As$ layer, which controls the potential barrier Φ_B. The dynamics can be described by a set of nonlinear differential equations for the spatially averaged carrier density n_1 in the GaAs layer, the parallel electric field $\mathscr{E}_\parallel$ and the potential barrier Φ_B [14].

The alteration in time of n_1 is expressed in the continuity equation

$$\dot{n}_1 = \frac{1}{e L_1}(J_{1\to 2} - J_{2\to 1}) \tag{1}$$

with the transversal thermionic-emission current densities given by Bethe's theory:

$$J_{1\to 2} = -e n_1 \sqrt{\frac{E_1}{3\pi m_1^*}} \exp\left(-\frac{3\Delta E_C}{2E_1}\right),$$

$$J_{2\to 1} = -e n_2 \sqrt{\frac{E_2}{3\pi m_2^*}} \exp\left(-\frac{3\Phi_B}{2E_2}\right),$$

where m_i^* are the effective masses and $E_i = \frac{3}{2} k_B T_i$ are the mean carrier energies given by the carrier temperatures T_i. The mean energy as a function of the applied electric field is estimated at $E_i \approx E_L + \tau_{E_i} e \mu_i \mathscr{E}_\parallel^2$, with the thermal equilibrium mean energy $E_L = \frac{3}{2} k_B T_L$, where T_L is the lattice temperature, and energy relaxation times τ_{E_i}. Because of local charge neutrality, the carrier density n_2 in the $Al_xGa_{1-x}As$ layer can be eliminated as a dependant variable: $n_2 = N_D - n_1 L_1/L_2$.

The dielectric relaxation of the parallel electric field is described by the equation

$$\varepsilon \dot{\mathscr{E}}_\parallel = -\sigma_L(\mathscr{E}_\parallel - \mathscr{E}_0) - \frac{e n_1 \mu_1 L_1 + e n_2 \mu_2 L_2}{L_1 + L_2} \mathscr{E}_\parallel \tag{2}$$

with $\sigma_L = d/[h(L_1 + L_2) R_L]$ and $\mathscr{E}_0 = U/d$. Here ε is the permittivity and R_L is the load resistance (see Figure 1).

The space charge in the $Al_xGa_{1-x}As$ layer results in an internal electric field $\mathscr{E}_\perp$ perpendicular to the layer, which is described by Poisson's equation $\varepsilon \partial \mathscr{E}_\perp(x,t)/\partial x = e(N_D - n(x))$ and the balance equation for the transverse current $\varepsilon \dot{\mathscr{E}}_\perp(x,t) + e\mu_2 n(x,t) \mathscr{E}_\perp(x,t) = 0$.

Bereitgestellt von | provisional account
Angemeldet
Heruntergeladen am | 14.11.18 14:53

For the dynamics of the potential barrier $\Phi_B = -e\int_0^{L_2} \mathscr{E}_\perp(x,t)\,dx$ we obtain the equation

$$\dot{\Phi}_B = \frac{e}{\varepsilon}\left(-\mu_2 N_D \Phi_B + \mu_2 \frac{e^2}{2\varepsilon} L_1^2 n_1^2\right). \quad (3)$$

Together, (1)–(3) describe the dynamics of real space transfer in the heterostructure.

3. Numerical Results

We have numerically simulated the dynamics of the system using the parameters in Table 1. Apart from self-generated periodic oscillations [14], the semiconductor can display chaotic oscillations if it is periodically driven by a bias voltage $U(t) = U_0 + U_{ac} \cdot \sin(2\pi f_d t)$. Figure 2 shows a phase portrait and a Poincaré section for the driven system. The strange attractor has the shape of a torus with a thickened, folded surface. In the Poincaré section four "wings" are visible, each in a different stage of the nonlinear folding mechanism. This kind of structure is typical for nonlinear oscillators with a periodic driving force [17] and is sometimes referred to as a Birkhoff-Shaw attractor.

We will now apply time-continuous chaos control to the driven system. This involves coupling the perpendicular voltage drop within the $Al_xGa_{1-x}As$ barrier Φ_B/e back to the dynamics of Φ_B, and may be realized by introducing a gate electrode on top of the GaAs layer to which the feedback signal $\delta\Phi_B$ is applied. The perturbation $\delta\Phi_B$ takes the specific form of the difference between the system output $\Phi_B(t)$ and the delayed output $\Phi_B(t-\tau)$ (*delayed feedback control*). The dynamics of the potential barrier is then given by

$$\dot{\Phi}_B = \frac{e}{\varepsilon}\left(-\mu_2 N_D \Phi_B + \mu_2 \frac{e^2}{2\varepsilon} L_1^2 n_1^2\right) + K\,\delta\Phi_B, \quad (4)$$

$$\delta\Phi_B(t) = [\Phi_B(t-\tau) - \Phi_B(t)]. \quad (5)$$

Here τ is a suitably chosen delay time and K is an experimentally adjustable perturbation weight. If $\Phi_B(t)$ is periodic with period τ, the difference term vanishes, and the system dynamics have the unperturbed form ($\delta\Phi_B = 0$). Therefore a UPO of the unperturbed system with period τ remains a solution if the control is switched on. The stabilization of this UPO can be achieved by an appropriate choice of K. This method has the advantage that the UPO need not to

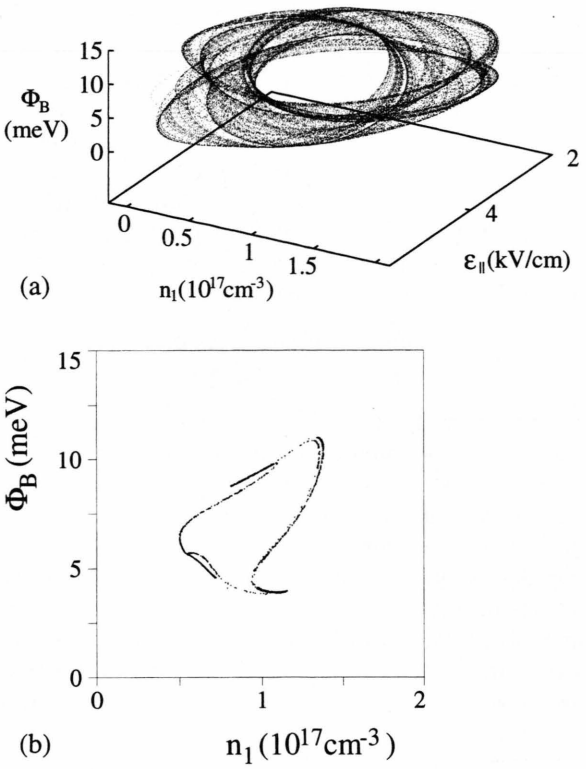

Fig. 2. The strange attractor of the driven real-space transfer oscillator. The numerical parameters are given in Table 1. (a) Phase portrait in the three-dimensional phase space of the dynamic variables $(n_1, \mathscr{E}_\parallel, \Phi_B)$. (b) Poincaré section of the potential barrier Φ_B and the carrier density n_1.

Table 1. Numerical parameters used in the simulation.

L_1	$=10$ nm	width of the GaAs layer [10]
L_2	$=20$ nm	width of the $Al_xGa_{1-x}As$ layer [10]
h	$=1$ mm	height of the device [10]
d	$=50$ μm	length of the device [10]
N_D	$=10^{17}$ cm^{-3}	effective donor concentration [10]
T_L	$=300$ K	temperature
ε	$=12\,\varepsilon_0$	permittivity [13]
ΔE_c	$=250$ meV	conduction band discontinuity
τ_{E_1}	$=1.8\cdot10^{-12}$ s	energy relaxation time in GaAs [15]
τ_{E_2}	$=6.4\cdot10^{-12}$ s	energy relaxation time in $Al_xGa_{1-x}As$ [15]
m_1^*	$=0.067\,m_0$	effective mass of the electrons in GaAs [13]
m_2^*	$=(0.067+0.3\cdot0.083)\,m_0$	effective mass of the electrons in $Al_xGa_{1-x}As$
μ_1	$=8000$ cm^2/Vs	electron mobility in GaAs [10]
μ_2	$=50$ cm^2/Vs	electron mobility in $Al_xGa_{1-x}As$ [16]
R_L	$=824\,\Omega$	load resistance
U_0	$=51.2$ V	dc bias
U_{ac}	$=2.5$ V	ac bias
f_d	$=293.2$ GHz	driving frequency

Bereitgestellt von | provisional account
Angemeldet
Heruntergeladen am | 14.11.18 14:53

be known explicitly. Experimentally, only a simple delay line is necessary. The disadvantage is that two control parameters, τ and K, have to be adjusted within a relatively small range to be determined empirically. The amplitude of the feedback signals $\delta\Phi_B(t)$ can be considered as a criterion for UPO stabilization. When the system moves along its UPO this amplitude is extremely small. We shall assume $\langle D^2(t)\rangle \ll 1$ as a criterion for stabilization, defining the dimensionless control signal $D(t)$ as follows:

$$D(t) \equiv \frac{\delta\Phi_B(t)}{\Phi_B^*} = \frac{[\Phi_B(t+\tau) - \Phi_B(t)]}{\Phi_B^*}, \tag{6}$$

where $\Phi_B^* \equiv 11.7$ meV has been chosen as reference value, and $\langle\ \rangle$ denotes the temporal average.

Figure 3 shows the stabilization of a period-five limit cycle. After the control signal is switched on at $t_c = 80$ ps, the amplitude $D(t)$ of the perturbation rapidly decays after a transient process and the system moves into the periodic regime corresponding to an initially unstable orbit of the unperturbed system. The delay time of the controlling feedback signal is equal to the period of the limit cycle, which gives an oscillation frequency of $f = 58.6$ GHz. This corresponds to 1/5 of the driving frequency f_d. Fig. 3(c) depicts the phase portrait for the post-transient regime. Comparison with Fig. 2(a) shows that the stabilized limit cycle is indeed embedded in the chaotic attractor of the unperturbed system.

By choosing a different delay time for the feedback signal, a different UPO can be stabilized for the same driving frequency and amplitude. Figure 4 shows the stabilization of a period-three UPO of the chaotic attractor, with an oscillation frequency of $f = 97.7$ GHz, corresponding to 1/3 of the driving frequency f_d. Here the control signal $D(t)$ does not run to zero but oscillates with a small amplitude. This effect is not expected in theory, and it is not yet well understood although it has been observed in numerical simulations of other systems [6, 18]. The fact that the effect is rather pronounced in this case may be due to the nature of the unperturbed system, which is periodically driven in time. However, the criterion for stabilization given above is satisfied.

Although the amplitude of perturbation becomes very small after a transient period, depending on initial conditions it can reach rather high values immediately after control is switched on. From the experimental point of view, it is undesirable that the accessible system parameter to which control is applied should experience strong bursts as shown in the simulations. Therefore we introduce a restriction to the delayed feedback signal as follows:

$$D(t) = \begin{cases} -D_0, & \text{when } K\,\delta\Phi_B(t) \le -D_0, \\ K\,\delta\Phi_B(t), & \text{when } -D_0 < K\,\delta\Phi_B(t) < D_0, \\ D_0, & \text{when } K\,\delta\Phi_B(t) \ge D_0. \end{cases} \tag{7}$$

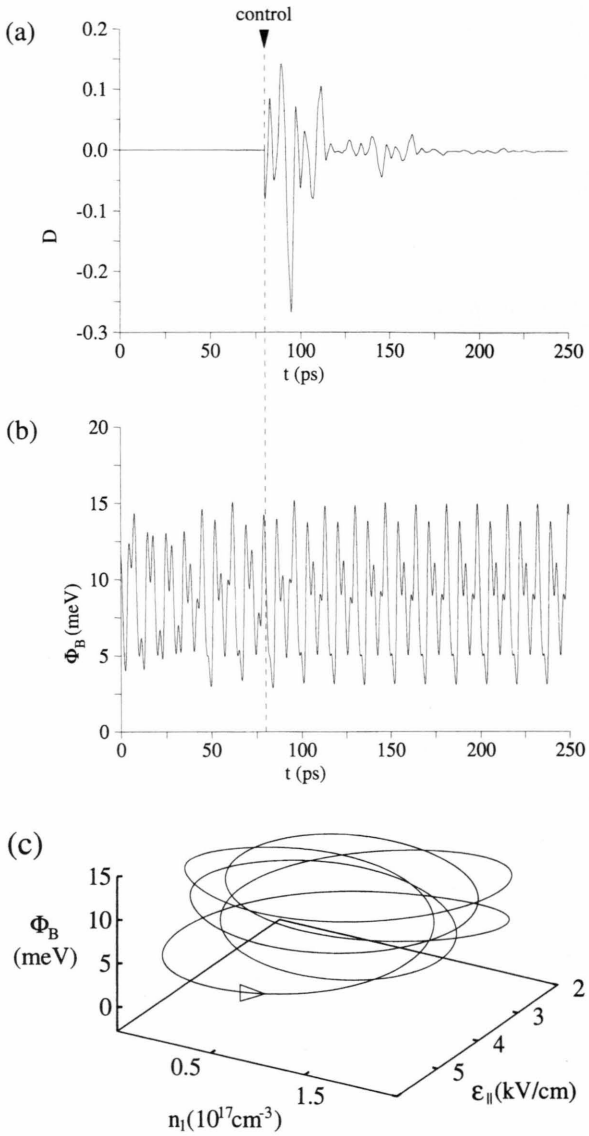

Fig. 3. Delayed feedback control: Stabilization of the period-five limit cycle. Time series for (a) the control signal, (b) the potential barrier. (Control is switched on at $t_c = 80$ ps; control parameters are $K = 0.1$ ps^{-1} and $\tau = 17.05$ ps.) (c) Phase portrait of the stabilized period-five limit cycle. Transient processes are omitted.

Bereitgestellt von | provisional account
Angemeldet
Heruntergeladen am | 14.11.18 14:53

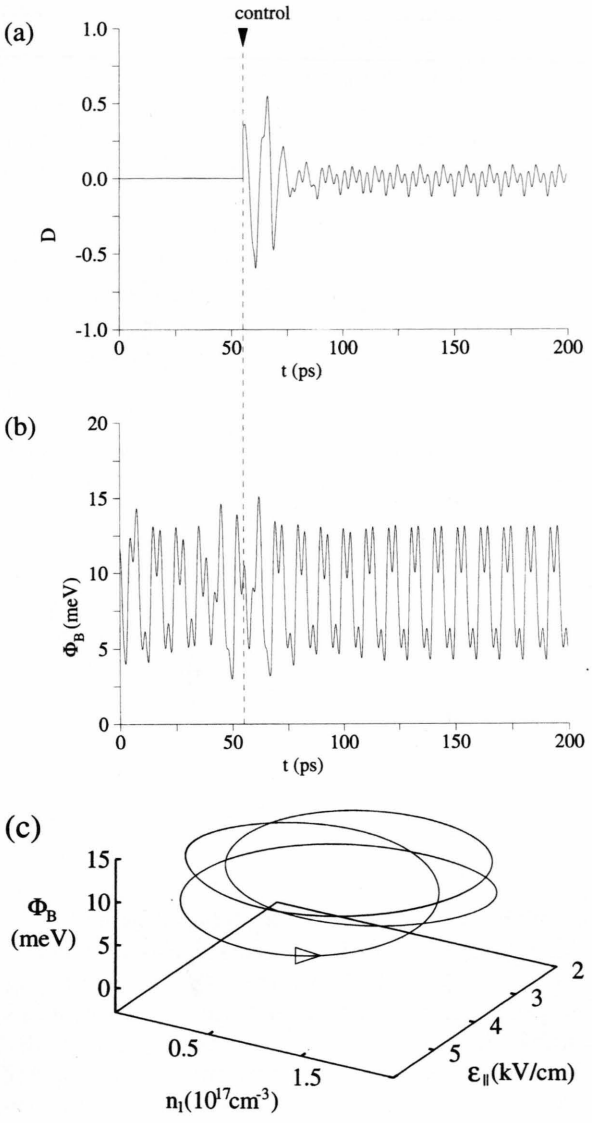

Fig. 4. Stabilization of the period-three limit cycle: Time series for (a) the control signal, (b) the potential barrier. (Control is switched on at $t_c = 50$ ps; control parameters are $K = 0.08\ \mathrm{ps}^{-1}$ and $\tau = 10.23$ ps.) (c) Phase portrait of the period-three limit cycle.

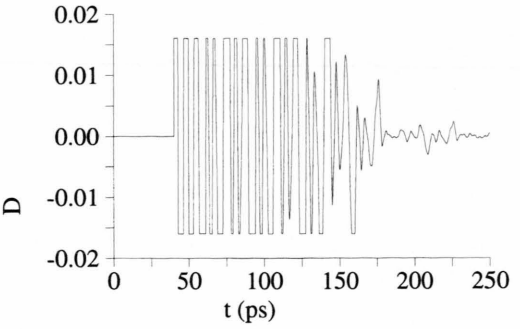

Fig. 5. Stabilization of the period-five limit cycle with restricted perturbation: Control signal $D(t)$ with $|D(t)| \leq D_0 = 0.016$. Control is switched on at $t_c = 40$ ps. Control parameters as in Figure 3.

Implementing this restriction in the physical system should be achieved by introducing some nonlinear electronic element in the feedback line so that the feedback signal reaches a saturation point at D_0. The effect of the restriction can be seen in Fig. 5 for the stabilization of the period-five limit cycle. Here the perturbation is small at all times, but the transient process is longer. The mean duration of the transient process increases with the decrease of D_0.

In general, unstable orbits are stabilized by the control only if τ and K are chosen appropriately. For a systematic investigation we consider the variance $\langle D^2(t)\rangle$ of the control signal. When the system moves along a UPO, the amplitude of the feedback signal and hence $\langle D^2(t)\rangle$ is small. The variance $\langle D^2(t)\rangle$ has been determined as a function of the coupling constant K for the two periodic orbits excluding transient processes in Figure 6. For both limit cycles a clear-cut interval for the value of K can be observed in which stabilization can easily be achieved. In both cases this interval is fairly wide and begins at rather low values for the coupling constant.

To further investigate the range in which K is suitable for stabilization of a given UPO, we have also calculated the largest non-zero Lyapunov exponent with respect to small deviations from the corresponding UPO. In Figure 7 the leading Lyapunov exponent λ is plotted as a function of the coupling constant for the period-five limit cycle. For $K_{min} = 0.10\ \mathrm{ps}^{-1} < K < K_{max} = 0.19\ \mathrm{ps}^{-1}$, $\lambda(K)$ is negative, i.e. the UPO is stabilized. If K is too small, the feedback is too weak for stabilization. If, on the other hand, K is too large, the controlled variable (Φ_B) changes so rapidly that the other (uncontrolled) dynamical variables cannot follow fast enough. Note that negative λ does not always imply that the UPO can be stabilized with a reasonably *small* control signal, as is evident from a comparison of Figs. 6(b) and 7.

When plotted as a function of the delay time τ, the variance $\langle D^2(t)\rangle$ exhibits a typical resonance struc-

Bereitgestellt von | provisional account
Angemeldet
Heruntergeladen am | 14.11.18 14:53

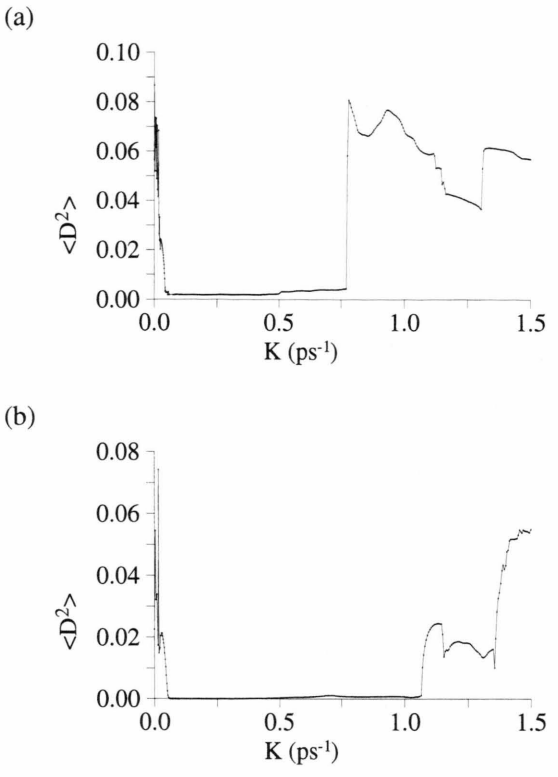

Fig. 6. Variance of the control amplitude as a function of coupling constant K: (a) for the period-three limit cycle ($\tau = 10.23$ ps) and (b) for the period-five limit cycle ($\tau = 17.05$ ps).

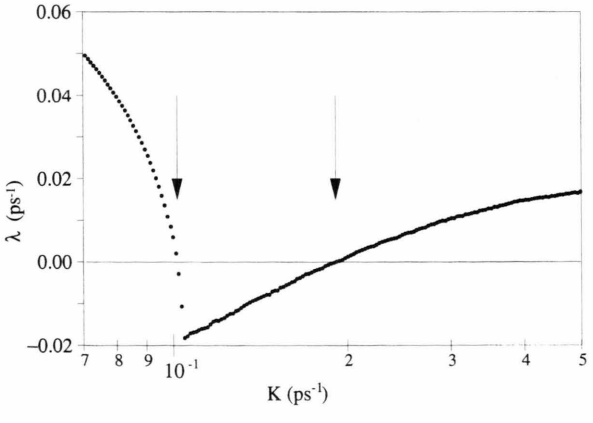

Fig. 7. The maximum non-negative Lyapunov exponent as a function of coupling constant K, calculated for the period-five limit cycle (delay time $\tau = 17.05$ ps). The arrows mark the absolute boundaries for stabilization.

ture (Fig. 8), with sharp minima at those values of τ which coincide with the period of a UPO. The resonance minimum of the period-five limit cycle is significantly deeper, corresponding to the better stabilization and stronger decay of the control signal (compare Figure 3(a)). Also we see a further minimum at $\tau = 2 \cdot 10.23$ ps.

In proximity of the resonance time $\tau = 17.05$ ps of the period-five limit cycle, the controlled system displays multistable behaviour. Two different asymptotic periodic orbits can be found for the same delay time, depending on initial conditions. Both branches of the graph are displayed in Figure 8. The lower branch is the minimum curve associated with stabilization of the period-five limit cycle. The upper branch is associated with an asymptotic period-three orbit together with large (non-decaying) perturbations. The presence of multistability in the controlled system is undesirable, and the problem can be avoided by using a restriction for the amplitude of the perturbation signal as given by (7). Figure 9 shows the effect of restriction on the resonance structure of $\langle D^2(t) \rangle$.

The plot is again made for different initial conditions: However, the upper branch at $\tau \approx 17$ ps has vanished and multistability is eliminated.

4. Conclusion

We have demonstrated that Pyragas' method of delayed feedback control represents an efficient and easily realizable method to turn undesired chaotic behaviour in nonlinear semiconductor oscillators into a stable mode of operation, which can be tuned in discrete steps. By choosing an appropriate delay time of the control signal, corresponding to an integer multiple of the driving period, quite different modes of self-generated periodic oscillations can be conveniently selected. Such flexibility cannot be achieved with a linear electronic oscillator, and we suggest that the occurrence of chaos thus offers useful applications in the field of hot electron devices. The same method has also been applied to control magnetic-field induced chaos [19] in a model of low-temperature impurity impact ionization breakdown in bulk semiconductors [20]. Here we have elaborated these ideas for an oscillation mechanism applicable to modulation-doped semiconductor heterostructures, as proposed in [21]. From a practical viewpoint those semiconductor structures are much more flexible, and hence poten-

Bereitgestellt von | provisional account
Angemeldet
Heruntergeladen am | 14.11.18 14:53

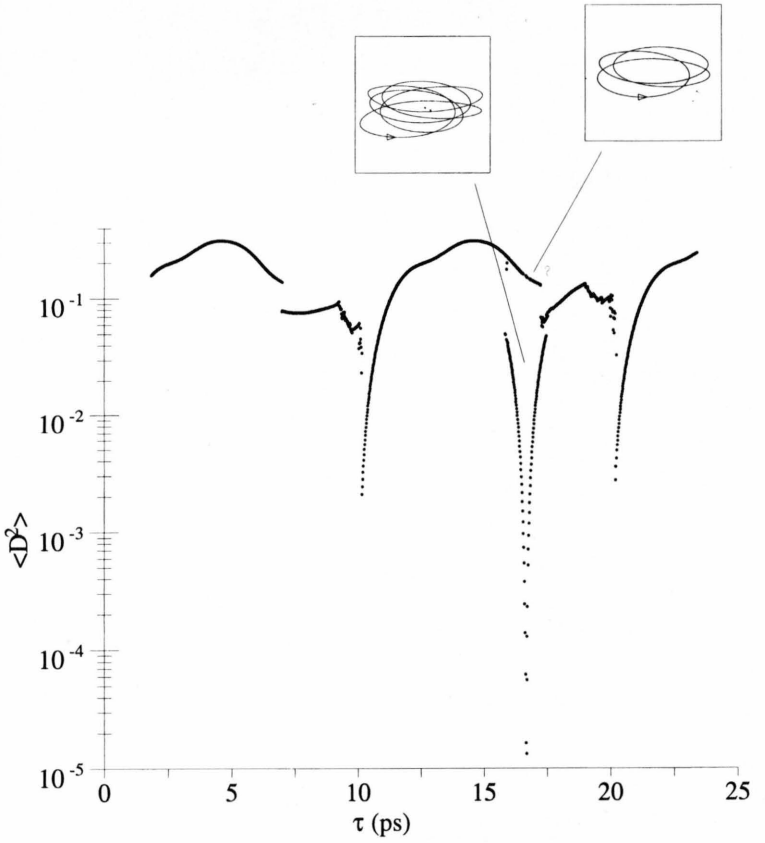

Fig. 8. Variance of the control amplitude as a function of delay time τ, plotted for different initial conditions. Multistability occurs around $\tau = 17$ ps. The coupling constant is $K = 0.1$ ps^{-1}, perturbation is unrestricted.

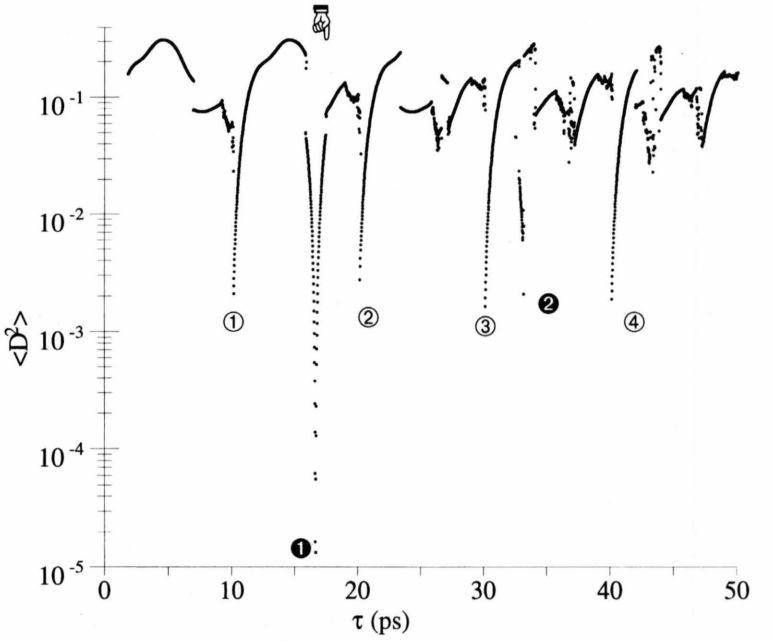

Fig. 9. Same as in Fig. 8, but the control signal is restricted to $|D(t)| \leq D_0 = 0.1$. The branch of multistability at $\tau = 17$ ps has disappeared. Further resonance points can be seen at integer multiples of 10.23 ps and 17.05 ps, numbered in white and black, respectively.

Bereitgestellt von | provisional account
Angemeldet
Heruntergeladen am | 14.11.18 14:53

tially useful, than bulk material. Finally we note that the stabilization of UPOs can also give insight into the dynamic structure of the uncontrolled chaotic system, since the UPOs constitute the "building bricks" of the chaotic attractor. The method of delayed feedback control can also be used to stabilize a UPO in a non-chaotic regime, and thus visualize, e.g., an unstable orbit which has appeared in a saddle-node bifurcation of two limit cycles.

Acknowledgements

We wish to thank R. Döttling and K. Pyragas for valuable discussions.

[1] E. Schöll, Nonequilibrium Phase Transitions in Semiconductors, Springer, Berlin 1987.
[2] E. Schöll, In Handbook of Semiconductors, ed. by P. T. Landsberg, 2nd ed., Elsevier, Amsterdam 1992.
[3] J. Peinke, J. Parisi, O. E. Rössler, and R. Stoop, Encounter with Chaos – Self-Organized Hierarchical Complexity in Semiconductors, Springer, Berlin 1992.
[4] M. P. Shaw, V. V. Mitin, E. Schöll, and H. L. Grubin, The Physics of Instabilities in Solid State Electron Devices, Plenum Press, New York 1992.
[5] E. Ott, C. Grebogi, and J. A. Yorke, Phys. Rev. Lett. **64,** 1196 (1990).
[6] K. Pyragas, Phys. Lett. A **170,** 421 (1992).
[7] M. Keever, H. Shichijo, K. Hess, S. Banerjee, L. Witowski, and H. Morkoc, Appl. Phys. Lett. **38,** 36 (1981).
[8] P. D. Coleman, J. Freeman, H. Morkoc, K. Hess, B. G. Streetman, and M. Keever, Appl. Phys. Lett. **40,** 493 (1982).
[9] N. Balkan and B. K. Ridley, Superlat. Microstr. **5,** 539 (1989).
[10] A. J. Vickers, A. Straw, and J. S. Roberts, Semicond. Sci. Technol. **4,** 743 (1989).
[11] P. Hendriks, E. A. E. Zwaal, J. G. A. Dubois, F. A. P. Blom, and J. H. Wolter, J. Appl. Phys. **69,** 302 (1991).
[12] N. Balkan, B. K. Ridley, and A. Vickers (eds.), Negative Differential Resistance and Instabilities in 2-D-Semiconductors, Plenum, New York 1993.
[13] E. Schöll and K. Aoki, Appl. Phys. Lett. **58,** 1277 (1991).
[14] R. Döttling and E. Schöll, Phys. Rev. B **45,** 1935 (1992).
[15] K. Hess and G. J. Iafrate, in Hot-Electron-Transport in Semiconductors, Topics in Applied Physics Vol. 58, ed. by L. Reggiani, Springer, Berlin 1985.
[16] H. Shichijo, K. Hess, and B. G. Streetman, Sol. State Electron. **23,** 817 (1980).
[17] R. Shaw, Z. Naturforsch. **36a,** 80 (1981).
[18] D. Reznik and E. Schöll, Z. Phys. B **91,** 309 (1993).
[19] G. Hüpper, A. Rein, and E. Schöll, Mod. Phys. Lett. B **6,** 1001 (1992).
[20] E. Schöll and K. Pyragas, Europhys. Lett. **24,** 159 (1993).
[21] E. Schöll, K. Pyragas, D. Cooper, and R. Döttling, Semicond. Sci. Technol. **9,** 559 (1994).

Bereitgestellt von | provisional account
Angemeldet
Heruntergeladen am | 14.11.18 14:53